

Coherent conversion between optical and microwave photons in Rydberg gases

Martin Kiffner^{1,2}, Amir Feizpour², Krzysztof T. Kaczmarek², Dieter Jaksch^{2,1}, and Joshua Nunn²
*Centre for Quantum Technologies, National University of Singapore, 3 Science Drive 2, Singapore 117543¹ and
 Clarendon Laboratory, University of Oxford, Parks Road, Oxford OX1 3PU, United Kingdom²*

Quantum information encoded in optical photons can be transmitted over long distances with very high information density, and suffers from negligible thermal noise at room temperature. On the other hand, microwave photons at cryogenic temperatures can be confined in high quality resonators and strongly coupled to solid-state qubits, providing a quantum bus to connect qubits and a route to deterministic photonic non-linearities. The coherent interconversion of microwave and optical photons has therefore recently emerged as a highly desirable capability that would enable freely-scalable networks of optically-linked qubits, or large-scale photonic information processing with multi-photon interactions mediated by microwaves. Here, we propose a route to efficient and coherent microwave-optical conversion based on frequency mixing in Rydberg atoms. The interaction requires no microfabricated components or cavities, and is tunable, broadband, and both spatially and spectrally multimode.

Bridging the microwave and optical domains enables the metrological transfer of atomic frequency standards [1], long-distance transmission of electronic data [2], and signal processing in radar and avionics [3]. Quantum computing via optically-mediated entanglement swapping [4–6] could also be enabled by coherent microwave-optical conversion (MOC) together with solid state systems such as spins in silicon [7] or superconducting qubits [8], which lack optical transitions (Fig. 1a). Josephson junctions can mediate microwave photonic non-linearities that cannot easily be replicated for optical photons [9] so that MOC also provides a route to freely-scalable all-photonic quantum computing (see Fig. 1b).

Recent MOC proposals have been based on optomechanical transduction [10, 11], or frequency mixing in Λ -type atomic ensembles [12–16]. Both approaches require high quality frequency-selective cavities limiting the conversion bandwidth, as well as aggressive cooling or optical pumping to bring the conversion devices into their quantum ground states.

In this paper, we propose instead to use frequency mixing in Rydberg gases for MOC (see Fig. 1c). The strong coupling between Rydberg atoms and microwaves has previously been used for detection and magnetometry [17–19], and cavity-mediated storage of microwaves in the ground state of a spin-cooled atomic ensemble has been analysed [20]. Here we show how to achieve efficient, broadband coherent MOC without the need for cavities, microfabrication or cooling. Our main result is a theoretical model establishing the principle of operation of the proposed device, which it is shown could be implemented in an ensemble of cold trapped Rb atoms.

Results

Conversion mechanism. Quantum information processing with microwave photons requires low ambient temperatures in order to suppress thermal background radiation. At such low temperatures it is appropriate to model the interaction of optical and microwave fields with an ensemble of cold trapped atoms, using the stan-

dard framework of coupled Maxwell-Bloch equations. A semi-classical analysis where the operator equations are solved numerically as c -number equations is appropriate because quantum fluctuations do not contribute to the conversion efficiency (see Methods). Our scheme does not require atom-atom interactions and operates in the low density regime where van der Waals interactions are negligible (see Supplementary Section ‘Interaction-induced imperfections’). The atomic level scheme is shown in Fig. 1c. We consider electric-dipole transitions between Rydberg states $|3\rangle$ and $|4\rangle$ with the same principal quantum number $n \gtrsim 25$. This transition couples strongly to the microwave field Ω_M of interest. The conversion between the microwave and the optical field Ω_L coupling to the $|1\rangle \leftrightarrow |6\rangle$ transition is accomplished via four auxiliary fields. The resonant fields Ω_P and Ω_R create a coherence on the $|1\rangle \leftrightarrow |3\rangle$ transition through coherent population trapping [21]. The two other auxiliary fields Ω_C and Ω_A link the microwave transition with the optical field Ω_L coupling to the $|6\rangle \leftrightarrow |1\rangle$ transition. The intensities and detunings of these fields are chosen such that a weak microwave field Ω_M creates a coherence on the optical transition $|6\rangle \leftrightarrow |1\rangle$, but not on the $|4\rangle \leftrightarrow |3\rangle$ transition. This quantum interference effect converts the microwave field into an optical field as it propagates through the medium. Similarly, a weak laser field Ω_L creates a coherence on the $|4\rangle \leftrightarrow |3\rangle$ transition without generating a coherence on the $|6\rangle \leftrightarrow |1\rangle$ transition, and hence it is converted into a microwave field. The conditions on the intensities and detunings of the auxiliary fields enabling this quantum interference effect are given by (see Supplementary Section ‘Analytical solution’)

$$|\Omega_R| \gg |\Omega_P|, \quad \Delta_5 = \frac{|\Omega_C|^2}{\Delta_4}, \quad \Delta_6 = \frac{|\Omega_A|^2}{\Delta_5}. \quad (1)$$

With these conditions, photon losses due to spontaneous emission are as small as possible thus enabling efficient and coherent MOC. Note that nearly lossless MOC in our scheme relies on the long lifetime of Rydberg states

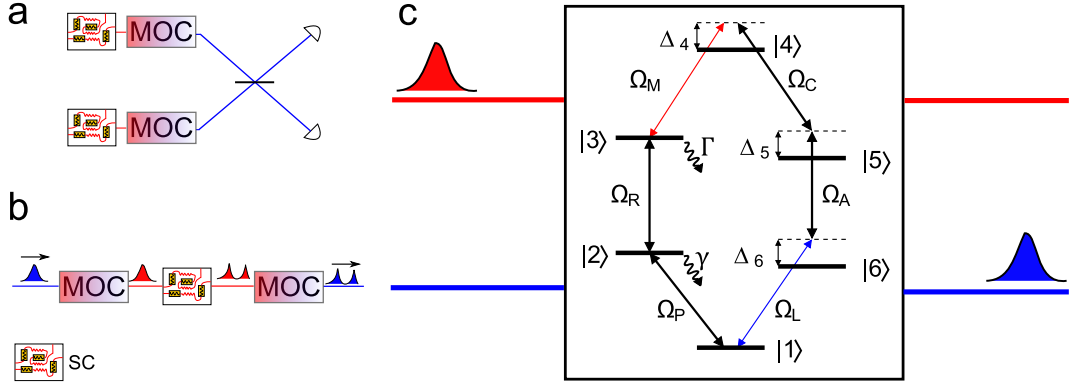


FIG. 1. **Applications of MOC and schematic drawing of our system.** **a** Entanglement swapping through microwave-optical conversion and efficient optical photon detectors. **b** Generation of entangled optical fields via microwave-optical conversion of strongly correlated microwave fields. The boxes labelled MOC and SC illustrate the conversion device and superconducting qubits, respectively. **c** Schematic drawing of the considered MOC device. A Microwave field (red) is coherently converted into an optical field (blue) through the interaction with cold atoms and vice versa. Transition frequencies and detunings shown in the atomic level scheme are not to scale. Ω_M and Ω_L are the Rabi frequencies associated with the microwave and the laser fields, respectively. Ω_P , Ω_R , Ω_C and Ω_A are Rabi frequencies of the auxiliary fields, and Δ_k is the detuning of the fields with state $|k\rangle$ ($k \in \{4, 5, 6\}$). Levels $|3\rangle$, $|4\rangle$ and $|5\rangle$ are Rydberg states with decay rate $\Gamma \ll \gamma$, where γ is the decay rate of states $|2\rangle$ and $|6\rangle$.

as shown below.

Stationary fields. In a first step we consider the interconversion of time-independent fields propagating along the z direction. Note that the transverse profile of the microwave must not necessarily be confined to the transverse size of the atom cloud, which can be challenging to achieve due to the large microwave wavelengths. If the transverse waist of the microwave beam exceeds the atomic cloud dimensions, the effective one-dimensional situation considered here can be realised by confining the microwave field to a waveguide such that its principal transverse electric mode significantly overlaps with the atomic cloud. We find that the spatial distribution of the microwave and optical fields $\Omega = (\Omega_M, \Omega_L)^t$ inside the medium is given by (see Supplementary Section ‘Analytical solution’),

$$\Omega(z) \approx e^{-\kappa z} \begin{pmatrix} \cos(kz) & ib \sin(kz) \\ \frac{i}{b} \sin(kz) & \cos(kz) \end{pmatrix} \Omega(0), \quad (2)$$

where $\kappa = (\varepsilon^2 + \varepsilon_\Gamma)/l_{\text{abs}}$ and $k = \varepsilon/l_{\text{abs}}$ determine the loss and the spatial oscillation period of the interconversion, respectively, and $l_{\text{abs}} = 1/(\mathcal{N}\sigma_L)$ is the resonant absorption length on the $|6\rangle \leftrightarrow |1\rangle$ transition (\mathcal{N} : atomic density, σ_L : absorption cross section). The dimensionless parameters ε and ε_Γ are defined as

$$\varepsilon = \frac{b}{4} \frac{\gamma}{|\Delta_4|} \frac{|\Omega_C|}{|\Omega_A|} \frac{|\Omega_P|}{|\Omega_R|}, \quad \varepsilon_\Gamma = \frac{\Gamma\gamma}{16|\Omega_A|^2} \left(1 + 2 \frac{|\Omega_C|^2}{\Delta_4^2} \right), \quad (3)$$

and we assumed $\varepsilon \ll 1$ and $\varepsilon_\Gamma/\varepsilon \ll 1$. The parameter $b = g_M/g_L$ in Eqs. (2) and (3) is the ratio of the single

photon Rabi frequencies g_M and g_L , where g_M (g_L) corresponds to the microwave (optical) transition (See ‘Methods’). In Eq. (2), the off-diagonal matrix element $(1, 2)$ $[(2, 1)]$ is proportional to b ($1/b$) since a single optical (microwave) photon with Rabi frequency g_L (g_M) gives rise to a Rabi frequency bg_L (g_M/b) on the microwave (optical) transition.

The spatial oscillations of optical and microwave intensities according to Eq. (2) are shown in Fig. 2. Our simple model is in excellent agreement with a full numerical solution of Maxwell-Bloch equations (see Methods). Complete MOC occurs after a length $L_c = \pi/(2k)$, and thus requires an optical depth $D_c = L_c/l_{\text{abs}}$ that is inversely proportional to ε in Eq. (3), $D_c = \pi/(2\varepsilon)$. Since the value of ε can be adjusted through the intensities and frequencies of the auxiliary fields, the condition for complete MOC can be met for various densities and sizes of atomic gases. In the example in Fig. 2, we find $L_c \approx 206.5l_{\text{abs}}$. The fidelity $F = e^{-2\kappa L_c}$ for complete conversion can be expressed in terms of the optical depth D_c ,

$$F(D_c) = \exp \left[-\frac{\pi^2}{2D_c} \right] \exp[-2\varepsilon_\Gamma D_c], \quad (4)$$

and $F(D_c)$ is shown in Fig. 3 for three different values of ε_Γ . The maximum fidelity $F_{\text{max}} = \exp(-2\pi\sqrt{\varepsilon_\Gamma})$ is attained at an optical depth $D_c^{\text{max}} = \pi/(2\sqrt{\varepsilon_\Gamma})$ and tends to unity for $\varepsilon_\Gamma \rightarrow 0$. Since $\varepsilon_\Gamma \propto \Gamma$, fidelities close to unity are only possible because of the slow radiative decay rate Γ of the Rydberg levels $|3\rangle$, $|4\rangle$ and $|5\rangle$. Γ decreases with increasing n as $\Gamma \propto n^{-3}$ [22] and is thus typically several orders of magnitude smaller than the decay rate γ of the low-lying states $|2\rangle$ and $|6\rangle$. The fidelity for complete

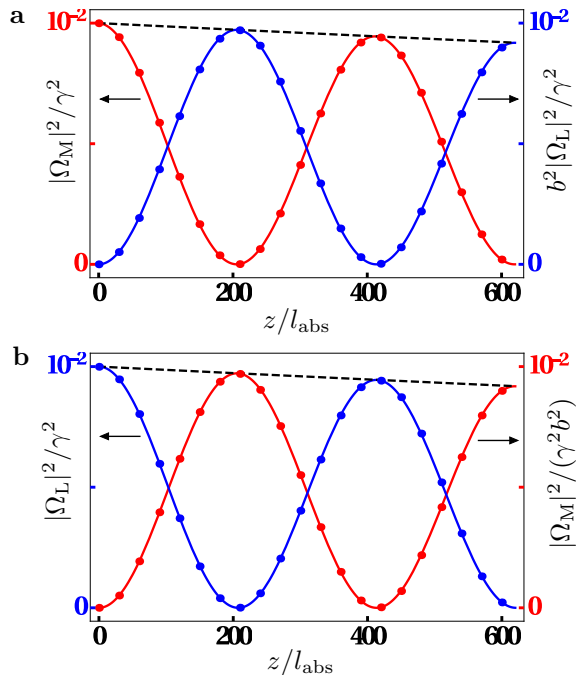


FIG. 2. **Frequency conversion of stationary fields.** Intensities of the microwave (red) and optical (blue) fields inside the medium. Dots indicate the results from a numerical integration of Maxwell-Bloch equations (see Methods). **a** A CW microwave field enters the medium at $z = 0$. **b** A CW optical field enters the medium at $z = 0$. In **a** and **b**, the dashed line is proportional to the envelope $e^{-2\kappa z}$ and we set $\Gamma/\gamma = 10^{-3}$, $\Omega_A = 3\gamma$, $\Omega_C = 2\gamma$, $\Omega_R = 3\gamma$, $\Omega_P = 0.1\gamma$, $\Delta_4 = 4\gamma$, $\Delta_5 = 1\gamma$, $\Delta_6 = 9\gamma$ and $b = \sqrt{30}$.

MOC for the parameters in Fig. 2 is $F \approx 97.2\%$. In the Supplementary Section ‘Example system’ we discuss a possible realisation of our level scheme in ^{87}Rb . We find that the fidelity for MOC and the required optical depth D_c for complete conversion are very similar to the results presented in Fig. 2.

Pulsed fields. Next we consider the conversion of pulsed fields. The derivation of Eq. (2) shows that our scheme is not mode-selective and works for broadband pulses (see Supplementary Section ‘Analytical solution’). The only requirement is that the atomic dynamics remains in the adiabatic regime, which holds if the bandwidth $\delta\nu$ of the input pulse is much smaller than all detunings Δ_k (see Fig. 1c). In order to demonstrate this, we present numerical solutions of Maxwell-Bloch equations for different microwave input pulses as shown in Fig. 4. The intensity of a microwave input pulse with Gaussian envelope is shown in Fig. 4a, and the corresponding optical output field is shown in Fig. 4b. In Fig. 4c we find that the shape of the optical output pulse matches the shape of the Gaussian input pulse very well. The distortionless conversion of a Gaussian input pulse with additional intensity oscillations is demonstrated in Fig. 4d. Finally, we note that

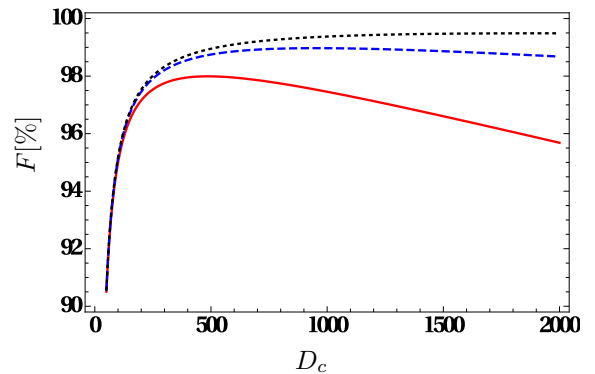


FIG. 3. **Conversion fidelity.** We set $\Gamma/\gamma = 10^{-3}$ (red solid line), $\Gamma/\gamma = 2.6 \times 10^{-4}$ (blue dashed line) and $\Gamma/\gamma = 6.4 \times 10^{-5}$ (black dotted line). These parameters correspond to Rubidium Rydberg states at zero temperature with $n \approx 30$, $n \approx 45$ and $n \approx 70$, respectively. Common parameters in all three curves are $\Omega_A = 3\gamma$, $\Omega_C = 2\gamma$ and $\Delta_4 = 4\gamma$.

the conversion of optical pulses to the microwave domain works equally well.

Discussion

We have shown that frequency mixing in Rydberg gases enables the coherent conversion between microwave and optical fields. The degree of conversion can be adjusted through the atomic density and the ancillary drive field intensities and frequencies. Complete conversion for travelling waves is achieved within a few hundred absorption lengths, and conversion fidelities of our scheme can exceed 99%. Our proposed MOC scheme enables the conversion of multiple frequency channels as required for multiplexed signals. The carrier frequency of these channels can be chosen from a broad spectrum of mm-waves due to the abundant possibilities for choosing the $|3\rangle \leftrightarrow |4\rangle$ transition within the Rydberg manifold. Atomic ensembles also provide for spatially multimode coherent interactions [23] and our free-space conversion scheme inherits this capability: multiple spatial channels or images could be directly converted. Cryostats with optical access are needed for solid-state-qubit optical networking, and these are being adapted to load cold atoms [24]. We are therefore optimistic that our scheme will provide the technically straightforward optical interface needed to achieve free-scaling quantum information processing.

METHODS

Maxwell-Bloch equations. A detailed derivation of the Maxwell-Bloch equations for our system is presented in the Supplementary Section ‘Model’. Here we present a short summary of the main equations. We model the time evolution of

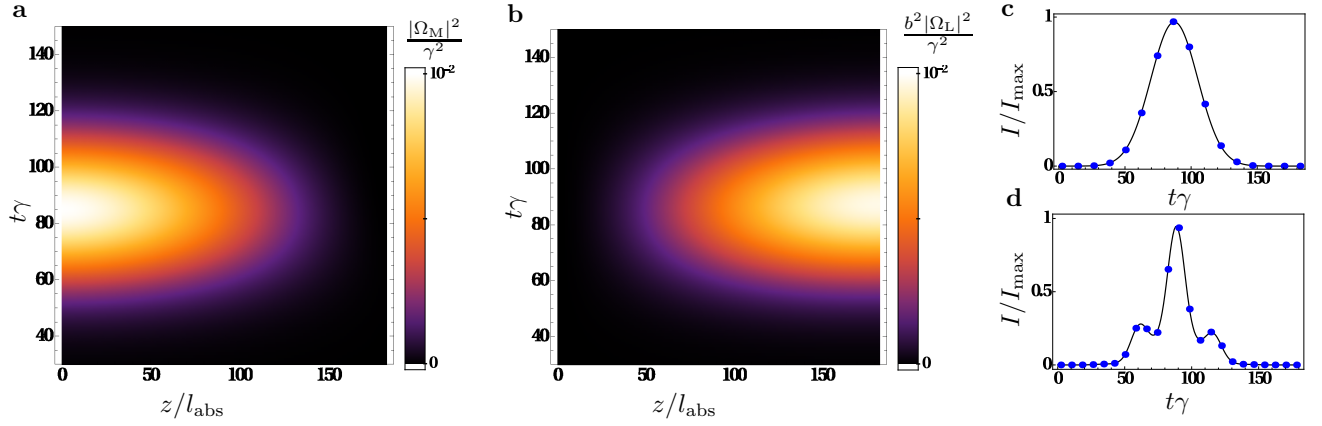


FIG. 4. **Frequency conversion of pulsed fields.** **a** Density plot of the incoming microwave pulse with a Gaussian envelope. **b** Density plot of the outgoing optical pulse. **c** Comparison between the intensity profile of the optical pulse at the medium output (blue solid line) and the shifted and re-scaled pulse shape of the incoming microwave field (blue dots). **d** Same as in **c**, but for a more general pulse shape. The parameters in **a-d** are $\Gamma/\gamma = 10^{-3}$, $\Omega_A = 4\gamma$, $\Omega_C = 6\gamma$, $\Omega_R = 3\gamma$, $\Omega_P = 0.1\gamma$, $\Delta_4 = 8\gamma$, $\Delta_5 = 4.5\gamma$, $\Delta_6 = 3.56\gamma$ and $b = \sqrt{30}$.

the atomic density operator by a Markovian master equation

$$\partial_t \varrho = -\frac{i}{\hbar} [H, \varrho] + \mathcal{L}_\gamma \varrho. \quad (5)$$

In electric-dipole and rotating-wave approximation, the Hamiltonian of each atom interacting with the six laser fields is

$$H = -\hbar \sum_{k=4}^6 \Delta_k A_{kk} - \hbar (\Omega_P A_{21} + \Omega_R A_{32} + \Omega_M A_{43} + \Omega_C A_{45} + \Omega_A A_{56} + \Omega_L A_{61} + \text{H.c.}), \quad (6)$$

where $A_{ij} = |i\rangle\langle j|$ are atomic transition operators. The six microwave and laser fields drive a resonant loop,

$$\omega_P + \omega_R + \omega_M - \omega_C - \omega_A - \omega_L = 0. \quad (7)$$

Since all fields are assumed to be co-propagating, this means that the phase matching condition is fulfilled. The term $\mathcal{L}_\gamma \varrho$ in Eq. (5) accounts for spontaneous emission of the excited states. These processes are described by standard Lindblad decay terms. The full decay rate of the states $|2\rangle$ and $|6\rangle$ is γ , and the long-lived Rydberg states decay with $\Gamma \ll \gamma$. The propagation of the probe and control fields inside the medium is governed by Maxwell's equations. For simplicity we only treat the microwave and laser field in a self-consistent way. In the slowly varying envelope approximation we find

$$\left(\frac{1}{c} \partial_t + \partial_z \right) \Omega_M = i\eta_M \varrho_{43}, \quad (8a)$$

$$\left(\frac{1}{c} \partial_t + \partial_z \right) \Omega_L = i\eta_L \varrho_{61}, \quad (8b)$$

and the coupling constants η_M and η_L are given by

$$\eta_M = \frac{\mathcal{N} |\mathbf{d}_{43}|^2}{2\hbar\epsilon_0 c} \omega_M, \quad (9a)$$

$$\eta_L = \frac{\mathcal{N} |\mathbf{d}_{61}|^2}{2\hbar\epsilon_0 c} \omega_L, \quad (9b)$$

and c is the speed of light. The ratio of the coupling constants can be expressed in terms of the ratio b of the single-photon Rabi frequencies defined in the main text, $\eta_M/\eta_L = (g_M/g_L)^2 = b^2$. The set of equations (5) and (8) represent a system of coupled, partial differential equations and have to be solved consistently for given initial and boundary conditions. We numerically solve the semi-classical system in Eqs. (5) and (8) using MATHEMATICA [25] and the implicit differential-algebraic solver (IDA) method option for NDSolve.

In our treatment the polarisation induced by the microwave and optical fields is linear in the Rabi frequencies Ω_M and Ω_L (see Supplementary section ‘Analytical solution’). Apart from quantum noise operators, our c-number calculations are thus equivalent to a Heisenberg-Langevin approach where the classical Rabi frequencies Ω_M and Ω_L are replaced by quantum fields [26–28]. Since the Langevin noise operators represent only vacuum noise, and do not contribute to the normally ordered expectation values determining the conversion efficiency, they can be dropped.

-
- [1] T. Fortier, M. Kirchner, F. Quinlan, J. Taylor, J. Bergquist, T. Rosenband, N. Lemke, A. Ludlow, Y. Jiang, C. Oates, *et al.*, Nat. Photon. **5**, 425 (2011)
 - [2] X. Yang, K. Xu, J. Yin, Y. Dai, F. Yin, J. Li, H. Lu, T. Liu, and Y. Ji, OPTEXP **22**, 869 (2014)
 - [3] M. Loïc, C. Stéphanie, F. Christian, C. Jean, M. Thomas, P. Gregoire, B. Ghaya, A. Mehdi, D. Daniel, B. Fabien, *et al.*, in *Radar Conference-Surveillance for a Safer World, 2009. RADAR. International* (IEEE, 2009) pp. 1–5
 - [4] S. D. Barrett and P. Kok, Phys. Rev. A **71**, 060310 (2005)
 - [5] C. Monroe, R. Raussendorf, A. Ruthven, K. Brown, P. Maunz, L.-M. Duan, and J. Kim, Phys. Rev. A **89**, 022317 (2014)

- [6] K. Nemoto, M. Trupke, S. J. Devitt, A. M. Stephens, B. Scharfenberger, K. Buczak, T. Nöbauer, M. S. Everitt, J. Schmiedmayer, and W. J. Munro, *Phys. Rev. X* **4**, 031022 (2014)
- [7] J. J. Morton and K. Mølmer, *Nature* **517**, 153 (2015)
- [8] R. Barendst, J. Kelly, A. Megrant, A. Veitia, D. Sank, E. Jeffrey, T. White, J. Mutus, A. Fowler, B. Campbell, Y. Chen, Z. Chen, B. Chiaro, A. Dunsworth, C. Neill, P. O'Malley, P. Roushan, A. Vainsencher, J. Wenner, A. N. Korotkov, A. N. Cleland, and J. M. Martinis, *Nature* **508**, 500 (2014)
- [9] A. Wallraff, D. I. Schuster, A. Blais, L. Frunzio, R.-S. Huang, J. Majer, S. Kumar, S. M. Girvin, and R. J. Schoelkopf, *Nature* **431**, 162 (2004)
- [10] R. Andrews, R. Peterson, T. Purdy, K. Cicak, R. Simmonds, C. Regal, and K. Lehnert, *Nat. Phys.* **10**, 321 (2014)
- [11] T. Bagci, A. Simonsen, S. Schmid, L. G. Villanueva, E. Zeuthen, J. Appel, J. M. Taylor, A. Sørensen, K. Usami, A. Schliesser, *et al.*, *Nature* **507**, 81 (2014)
- [12] L. A. Williamson, Y.-H. Chen, and J. J. Longdell, *Phys. Rev. Lett.* **113**, 203601 (2014)
- [13] C. O'Brien, N. Lauk, S. Blum, G. Morigi, and M. Fleischhauer, *Phys. Rev. Lett.* **113**, 063603 (2014)
- [14] S. Blum, C. O'Brien, N. Lauk, P. Bushev, M. Fleischhauer, and G. Morigi, *Phys. Rev. A* **91**, 033834 (2015)
- [15] M. Hafezi, Z. Kim, S. Rolston, L. Orozco, B. Lev, and J. Taylor, *Phys. Rev. A* **85**, 020302 (2012)
- [16] D. Marcos, M. Wubs, J. Taylor, R. Aguado, M. Lukin, and A. S. Sørensen, *Phys. Rev. Lett.* **105**, 210501 (2010)
- [17] J. A. Sedlacek, A. Schwettmann, H. Kübler, R. Löw, T. Pfau, and J. P. Shaffer, *Nat. Phys.* **8**, 819 (2012)
- [18] J. A. Gordon, C. L. Holloway, A. Schwarzkopf, D. A. Anderson, S. Miller, N. Thaicharoen, and G. Raithel, *Appl. Phys. Lett.* **105**, 024104 (2014)
- [19] H. Fan, S. Kumar, J. Sedlacek, H. Kübler, S. Karimkashi, and J. P. Shaffer, *J. Phys. B* **48**, 202001 (2015)
- [20] D. Petrosyan, G. Bentsky, G. Kurizki, I. Mazets, J. Majer, and J. Schmiedmayer, *Phys. Rev. A* **79**, 040304(R) (2009)
- [21] E. Arimondo, in E. Wolf (Ed.), *Progress in Optics*, Vol. **35**, pp. 258, Elsevier, Amsterdam (1996).
- [22] I. I. Beterov, I. I. Ryabtsev, D. B. Tretyakov, and V. M. Entin, *Phys. Rev. A* **79**, 052504 (2009)
- [23] D. B. Higginbottom, B. M. Sparkes, M. Rancic, O. Pinel, M. Hosseini, P. K. Lam, and B. C. Buchler, *Phys. Rev. A* **86**, 023801 (2012)
- [24] D. Cano, H. Hattermann, B. Kasch, C. Zimmermann, R. Kleiner, D. Koelle, and J. Fortágh, *Eur. Phys. J. D* **63**, 17 (2011)
- [25] Wolfram Research, Inc., *Mathematica Version 10.1* (Wolfram Research, Inc., Irvine, Champaign, Illinois)
- [26] M. Fleischhauer and M. D. Lukin, *Phys. Rev. A* **65**, 022314 (2002)
- [27] M. Hafezi, D. E. Chang, V. Gritsev, E. Demler, and M. Lukin, *Phys. Rev. B* **85**, 013822 (2012)
- [28] F. E. Zimmer, J. Otterbach, R. G. Unanyan, B. W. Shore, and M. Fleischhauer, *Phys. Rev. A* **77**, 063823 (2008)

ACKNOWLEDGMENTS

MK thanks the National Research Foundation and the Ministry of Education of Singapore for support. The

research leading to these results has received financial support from the European Research Council under the European Union's Seventh Framework Programme (FP7/2007-2013)/ERC Grant Agreement no. 319286 (Q-MAC).

AUTHOR CONTRIBUTIONS

MK conceived the project and modelled the system. All authors contributed to the development of the scheme and wrote the manuscript.

COMPETING FINANCIAL INTERESTS

The authors declare no competing financial interests.

Supplementary Material for: Coherent conversion between optical and microwave photons in Rydberg gases

*Martin Kiffner^{1,2}, Amir Feizpour², Krzysztof T. Kaczmarek², Dieter Jaksch^{2,1}, Joshua Nunn²
Centre for Quantum Technologies, National University of Singapore, 3 Science Drive 2, Singapore 117543¹
Clarendon Laboratory, University of Oxford, Parks Road, Oxford OX1 3PU, United Kingdom²

MODEL

Here we derive the Maxwell-Bloch equations for our system from first principles. The electric field amplitude of the microwave field is \mathbf{E}_M , and the optical field is denoted by \mathbf{E}_L . The other fields \mathbf{E}_P , \mathbf{E}_R and \mathbf{E}_C are auxiliary fields facilitating the frequency conversion. We decompose all electric fields as ($X \in \{P, R, M, C, L\}$)

$$\mathbf{E}_X = \mathbf{E}_X^{(+)}(\mathbf{r}, t) + \text{c.c.}, \quad (10)$$

where $\mathbf{E}_X^{(+)}$ is the positive frequency part of field X . The positive frequency parts of \mathbf{E}_M and \mathbf{E}_L are defined as

$$\mathbf{E}_M^{(+)}(\mathbf{r}, t) = \mathbf{e}_M \mathcal{E}_M(\mathbf{r}, t) e^{i(\mathbf{k}_M \cdot \mathbf{r} - \omega_M t)}, \quad (11a)$$

$$\mathbf{E}_L^{(+)}(\mathbf{r}, t) = \mathbf{e}_L \mathcal{E}_L(\mathbf{r}, t) e^{i(\mathbf{k}_L \cdot \mathbf{r} - \omega_L t)}, \quad (11b)$$

where \mathbf{e}_M (\mathbf{e}_L) is the unit polarisation vector, ω_M (ω_L) is the central frequency, \mathbf{k}_M (\mathbf{k}_L) is the wave vector and \mathcal{E}_M (\mathcal{E}_L) is the envelope function of \mathbf{E}_M (\mathbf{E}_L). The positive frequency parts of the auxiliary fields are given by

$$\mathbf{E}_P^{(+)}(\mathbf{r}, t) = \mathbf{e}_P \mathcal{E}_P e^{i(\mathbf{k}_P \cdot \mathbf{r} - \omega_P t)}, \quad (12a)$$

$$\mathbf{E}_R^{(+)}(\mathbf{r}, t) = \mathbf{e}_R \mathcal{E}_R e^{i(\mathbf{k}_R \cdot \mathbf{r} - \omega_R t)}, \quad (12b)$$

$$\mathbf{E}_C^{(+)}(\mathbf{r}, t) = \mathbf{e}_C \mathcal{E}_C e^{i(\mathbf{k}_C \cdot \mathbf{r} - \omega_C t)}, \quad (12c)$$

$$\mathbf{E}_A^{(+)}(\mathbf{r}, t) = \mathbf{e}_A \mathcal{E}_A e^{i(\mathbf{k}_A \cdot \mathbf{r} - \omega_A t)}, \quad (12d)$$

where \mathbf{e}_X , \mathcal{E}_X and ω_X is the unit polarisation vector, envelope function and central frequency of field \mathbf{E}_X , respectively ($X \in \{P, R, C, A\}$). In order to simplify the notation, we introduce atomic transition operators

$$A_{ij} = |i\rangle\langle j|, \quad A_{ij}^\dagger = A_{ji}. \quad (13)$$

In electric-dipole and rotating-wave approximation, the Hamiltonian of each atom interacting with the six laser fields is

$$\begin{aligned} H = & \hbar \sum_{k=2}^5 \omega_k A_{kk} - \left(A_{21} \mathbf{d}_{21} \cdot \mathbf{E}_P^{(+)} + A_{32} \mathbf{d}_{32} \cdot \mathbf{E}_R^{(+)} \right. \\ & + A_{43} \mathbf{d}_{43} \cdot \mathbf{E}_M^{(+)} + A_{45} \mathbf{d}_{45} \cdot \mathbf{E}_C^{(+)} \\ & \left. + A_{56} \mathbf{d}_{56} \cdot \mathbf{E}_A^{(+)} + A_{61} \mathbf{d}_{61} \cdot \mathbf{E}_L^{(+)} + \text{H.c.} \right), \quad (14) \end{aligned}$$

where ω_k denotes the energy of state $|k\rangle$ with respect to the energy of level $|1\rangle$. The matrix element of the electric

dipole moment operator $\hat{\mathbf{d}}$ on the transition transition $|i\rangle \leftrightarrow |j\rangle$ is defined as

$$\mathbf{d}_{ij} = \langle i | \hat{\mathbf{d}} | j \rangle. \quad (15)$$

We model the time evolution of the atomic system by a master equation for the reduced density operator R ,

$$\partial_t R = -\frac{i}{\hbar} [H, R] + \mathcal{L}_\gamma R. \quad (16)$$

The last term in Eq. (16) describes spontaneous emission and is given by

$$\begin{aligned} \mathcal{L}_\gamma R = & -\frac{\gamma}{2} \left(A_{12}^\dagger A_{12} R + R A_{12}^\dagger A_{12} - 2 A_{12} R A_{12}^\dagger \right) \\ & -\frac{\Gamma}{2} \left(A_{23}^\dagger A_{23} R + R A_{23}^\dagger A_{23} - 2 A_{23} R A_{23}^\dagger \right), \\ & -\frac{\Gamma}{2} \left(A_{34}^\dagger A_{34} R + R A_{34}^\dagger A_{34} - 2 A_{34} R A_{34}^\dagger \right), \\ & -\frac{\Gamma}{2} \left(A_{54}^\dagger A_{54} R + R A_{54}^\dagger A_{54} - 2 A_{54} R A_{54}^\dagger \right), \\ & -\frac{\Gamma}{2} \left(A_{65}^\dagger A_{65} R + R A_{65}^\dagger A_{65} - 2 A_{65} R A_{65}^\dagger \right). \\ & -\frac{\gamma}{2} \left(A_{16}^\dagger A_{16} R + R A_{16}^\dagger A_{16} - 2 A_{16} R A_{16}^\dagger \right). \end{aligned}$$

While the ground states $|1\rangle$ is assumed to be (meta-) stable, the states $|2\rangle$, $|3\rangle$, $|4\rangle$ and $|5\rangle$ decay through spontaneous emission. The decay rate γ is the full decay rate of states $|2\rangle$ and $|5\rangle$, and Γ is the decay rate on the Rydberg transitions. In our scheme, Γ is much smaller than the decay rate γ of the low-lying electronic states. In order to remove the fast oscillating terms in Eq. (16), we transform the latter equation into a rotating frame

$$\begin{aligned} W = & \exp \{ i[\omega_P A_{22} + (\omega_P + \omega_R) A_{33} \\ & + (\omega_P + \omega_R + \omega_M) A_{44} \\ & + (\omega_P + \omega_R + \omega_M - \omega_C) A_{55} \\ & + (\omega_P + \omega_R + \omega_M - \omega_C - \omega_A) A_{66}] t \} \\ & \exp \{ -i[\mathbf{k}_P \cdot \mathbf{r} A_{22} + (\mathbf{k}_P + \mathbf{k}_R) \cdot \mathbf{r} A_{33} \\ & + (\mathbf{k}_P + \mathbf{k}_R + \mathbf{k}_M) \cdot \mathbf{r} A_{44} \\ & + (\mathbf{k}_P + \mathbf{k}_R + \mathbf{k}_M - \mathbf{k}_C) \cdot \mathbf{r} A_{55}] \\ & + (\mathbf{k}_P + \mathbf{k}_R + \mathbf{k}_M - \mathbf{k}_C - \mathbf{k}_A) \cdot \mathbf{r} A_{66} \} \}. \end{aligned}$$

We assume that the central frequencies of all fields are resonant with the loop $|1\rangle \leftrightarrow |2\rangle \leftrightarrow |3\rangle \leftrightarrow |4\rangle \leftrightarrow |5\rangle \leftrightarrow |6\rangle \leftrightarrow |1\rangle$,

$$\omega_P + \omega_R + \omega_M - \omega_C - \omega_A = \omega_L. \quad (17)$$

In addition, we impose the phase matching condition

$$\mathbf{k}_P + \mathbf{k}_R + \mathbf{k}_M - \mathbf{k}_C - \mathbf{k}_A = \mathbf{k}_L. \quad (18)$$

For co-propagating fields as considered in the main text, Eq. (17) implies Eq. (18). The transformed density operator $\varrho = WRW^\dagger$ obeys the master equation

$$\partial_t \varrho = -\frac{i}{\hbar} [H', \varrho] + \mathcal{L}_\gamma \varrho, \quad (19)$$

and the transformed Hamiltonian H' is

$$H' = -\hbar \sum_{k=4}^6 \Delta_k A_{kk} - \hbar (\Omega_P A_{21} + \Omega_R A_{32} + \Omega_M A_{43} + \Omega_C A_{45} + \Omega_A A_{56} + \Omega_L A_{61} + \text{H.c.}) . \quad (20)$$

In this equation, Δ_k $k \in \{2, \dots, 6\}$ is a detuning defined as

$$\Delta_4 = \omega_P + \omega_R + \omega_M - \omega_4, \quad (21a)$$

$$\Delta_5 = \omega_P + \omega_R + \omega_M - \omega_C - \omega_5, \quad (21b)$$

$$\Delta_6 = \omega_L - \omega_6. \quad (21c)$$

The Rabi frequencies of the various fields are

$$\Omega_P = \frac{\mathbf{d}_{21} \cdot \mathbf{e}_P}{\hbar} \mathcal{E}_P, \quad (22a)$$

$$\Omega_R = \frac{\mathbf{d}_{32} \cdot \mathbf{e}_R}{\hbar} \mathcal{E}_R, \quad (22b)$$

$$\Omega_M = \frac{\mathbf{d}_{43} \cdot \mathbf{e}_M}{\hbar} \mathcal{E}_M, \quad (22c)$$

$$\Omega_C = \frac{\mathbf{d}_{45} \cdot \mathbf{e}_C}{\hbar} \mathcal{E}_C, \quad (22d)$$

$$\Omega_A = \frac{\mathbf{d}_{45} \cdot \mathbf{e}_A}{\hbar} \mathcal{E}_A, \quad (22e)$$

$$\Omega_L = \frac{\mathbf{d}_{51} \cdot \mathbf{e}_L}{\hbar} \mathcal{E}_L. \quad (22f)$$

Since Ω_M and Ω_L depend on position and time via the envelope functions \mathcal{E}_M and \mathcal{E}_L , the density operator ϱ in the rotating frame is a slowly varying function of \mathbf{r} and t . The propagation of the probe and control fields inside the medium is governed by Maxwell's equations. We only take into account \mathbf{E}_M and \mathbf{E}_L for the self-consistent Maxwell-Bloch equations. The P and R fields create coherent population trapping on the $|1\rangle \leftrightarrow |2\rangle \leftrightarrow |3\rangle$ transition such that the atoms are in a dark state for these fields. After a transient time, the P and R fields will thus not experience absorption or dispersion. Furthermore, the auxiliary fields C and A are detuned from resonance and couple to states that are virtually empty (see Supplementary Section 'Analytical solution'). We can thus neglect their absorption and dispersion. The wave equation governing the propagation of the electric field $\mathbf{E} = \mathbf{E}_M + \mathbf{E}_L$ is then given by

$$\left(\frac{1}{c^2} \partial_t^2 - \Delta \right) \mathbf{E} = -\frac{1}{c^2 \epsilon_0} \partial_t^2 \mathbf{P}. \quad (23)$$

The source term on the right hand side of Eq. (23) comprises the macroscopic polarisation \mathbf{P} induced by the microwave and optical fields. If atom-atom interactions can be neglected (see Supplementary Section 'Interaction-induced imperfections'), \mathbf{P} can be expressed in terms of the single-atom polarisation,

$$\mathbf{P} = \mathcal{N}(\mathbf{d}_{34} R_{43} + \mathbf{d}_{16} R_{61} + \text{c.c.}). \quad (24)$$

In this equation, \mathcal{N} is the mean atomic density of the medium. Note that the coherences R_{43} and R_{61} in Eq. (24) are related to the coherences of the density operator ϱ in the rotating frame by

$$R_{43} = \varrho_{43} e^{i(\mathbf{k}_M \cdot \mathbf{r} - \omega_M t)}, \quad R_{61} = \varrho_{61} e^{i(\mathbf{k}_L \cdot \mathbf{r} - \omega_L t)}. \quad (25)$$

In the slowly varying envelope approximation [1] and with Eqs. (11) and (22), the wave equation (23) can be cast into the form

$$\left(\frac{1}{c} \partial_t + \hat{\mathbf{k}}_M \cdot \nabla \right) \Omega_M = i \eta_M \varrho_{43}, \quad (26a)$$

$$\left(\frac{1}{c} \partial_t + \hat{\mathbf{k}}_L \cdot \nabla \right) \Omega_L = i \eta_L \varrho_{61}, \quad (26b)$$

where $\hat{\mathbf{k}}_X = \mathbf{k}_X / k_X$ denote unit vectors. The coupling constants η_M and η_L are given by

$$\eta_M = \frac{\mathcal{N} |\mathbf{d}_{43}|^2}{2 \hbar \epsilon_0 c} \omega_M, \quad (27a)$$

$$\eta_L = \frac{\mathcal{N} |\mathbf{d}_{61}|^2}{2 \hbar \epsilon_0 c} \omega_L, \quad (27b)$$

and c is the speed of light. In the case of η_L it is useful to replace the dipole moment through the radiative decay rate,

$$\eta_L = \frac{3 \mathcal{N} \lambda_{61}^2}{8 \pi} \gamma_{61}, \quad (28)$$

where λ_{61} is the wavelength of the atomic transition $|6\rangle \leftrightarrow |1\rangle$.

The ratio η_M / η_L is equal to the ratio of the single-photon Rabi frequencies defined in the main text,

$$\frac{\eta_M}{\eta_L} = \frac{|\mathbf{d}_{43}|^2 \omega_M}{|\mathbf{d}_{61}|^2 \omega_L} = \left(\frac{g_M}{g_L} \right)^2 = b^2. \quad (29)$$

Finally, we show that the coupling parameter η_M corresponding to the microwave field can be much larger than η_L . To this end we note that transition energies between Rydberg states with the same principal quantum number n and different angular momenta are given by

$$\begin{aligned} (E_{nl_j} - E_{nl_{j'}}) / E_{Ry} &= -\frac{1}{(n - \delta_{l_j})^2} + \frac{1}{(n - \delta_{l_{j'}})^2} \\ &= -\frac{\delta_{l_j}^2 - \delta_{l_{j'}}^2 - 2n(\delta_{l_j} - \delta_{l_{j'}})}{(n - \delta_{l_j})^2 (n - \delta_{l_{j'}})^2} \\ &\approx 2 \frac{\delta_{l_{j'}} - \delta_{l_j}}{n^3}, \quad n \gg 1, \end{aligned} \quad (30)$$

where E_{Ry} is the Rydberg energy and δ_{l_j} ($\delta_{l'_j}$) is the quantum defect of angular momentum state nl_j (nl'_j). In addition, the electric-dipole moment on the $|3\rangle \leftrightarrow |4\rangle$ transition scales as follows [2, 3],

$$|\mathbf{d}_{43}|^2 \propto n^4, \quad n \gg 1. \quad (31)$$

Combining Eqs. (30) and (31) we find $|\mathbf{d}_{43}|^2 \omega_{\text{M}} \propto n$, and hence $\eta_{\text{M}}/\eta_{\text{L}} \propto n$. This shows that η_{M} can be much larger than η_{L} for highly excited Rydberg states.

ANALYTICAL SOLUTION

Here we outline the analytical solution to the Maxwell-Bloch equations of our system. In a first step, we derive the adiabatic solutions for the atomic coherences on the microwave and optical transitions in Sec. . Second, we employ this result to find an analytical solution to the Maxwell-Bloch equations for stationary fields in Sec. .

Atomic coherences

In order to obtain approximate expressions for the coherences ϱ_{43} and ϱ_{61} , we assume that the fields Ω_{M} and Ω_{L} are sufficiently weak and expand the atomic density operator as follows [4, 5],

$$\varrho = \sum_{k=0}^{\infty} \varrho^{(k)}, \quad (32)$$

where $\varrho^{(k)}$ denotes the contribution to ϱ in k th order in the Hamiltonian

$$H_1 = -\hbar(\Omega_{\text{M}}A_{43} + \Omega_{\text{L}}A_{61}) + \text{H.c.} \quad (33)$$

The solutions $\varrho^{(k)}$ can be obtained by re-writing the master equation (19) as

$$\mathcal{L}\varrho = \mathcal{L}_0\varrho - \frac{i}{\hbar}[H_1, \varrho], \quad (34)$$

where the linear super-operator \mathcal{L}_0 is independent of Ω_{M} and Ω_{L} . Inserting the expansion (32) into Eq. (34) leads to the following set of coupled differential equations

$$\dot{\varrho}^{(0)} = \mathcal{L}_0\varrho^{(0)}, \quad (35)$$

$$\dot{\varrho}^{(k)} = \mathcal{L}_0\varrho^{(k)} - \frac{i}{\hbar}[H_1, \varrho^{(k-1)}], \quad k > 0. \quad (36)$$

Equation (35) describes the interaction of the atom with the fields Ω_{P} , Ω_{R} , Ω_{C} and Ω_{A} to all orders and in the absence of H_1 . Higher-order contributions to ϱ can be obtained if Eq. (36) is solved iteratively. Equations (35) and (36) must be solved under the constraints $\text{Tr}(\varrho^{(0)}) = 1$ and $\text{Tr}(\varrho^{(k)}) = 0$ ($k > 0$).

We omit the small decay rate Γ of state $|3\rangle$ and find that the zeroth order solution in steady state is given by the EIT dark state of the three-level ladder system $|1\rangle$, $|2\rangle$ and $|3\rangle$,

$$\varrho_{11}^{(0)} = P_{11} = \frac{|\Omega_{\text{R}}|^2}{|\Omega_{\text{P}}|^2 + |\Omega_{\text{R}}|^2}, \quad (37a)$$

$$\varrho_{33}^{(0)} = P_{33} = \frac{|\Omega_{\text{P}}|^2}{|\Omega_{\text{P}}|^2 + |\Omega_{\text{R}}|^2}, \quad (37b)$$

$$\varrho_{13}^{(0)} = C_{13} = -\frac{\Omega_{\text{P}}^* \Omega_{\text{R}}}{|\Omega_{\text{P}}|^2 + |\Omega_{\text{R}}|^2}. \quad (37c)$$

For $|\Omega_{\text{P}}| \ll |\Omega_{\text{R}}|$ the steady state is reached within several inverse decay times $1/\gamma$. Next we solve Eq. (36) for $k = 1$ and obtain

$$\begin{aligned} \varrho^{(1)}(t) = & \frac{i}{\hbar} \mathcal{L}_0^{-1} [H_1(t), \varrho^{(0)}] \\ & - \frac{i}{\hbar} \mathcal{L}_0^{-1} \int_0^t dt' e^{\mathcal{L}_0(t-t')} \partial_{t'} \left([H_1(t'), \varrho^{(0)}] \right), \end{aligned} \quad (38)$$

where we assumed $H_1(0) = 0$. If $H_1(t)$ varies sufficiently slowly with time, the second term on the right-hand side in Eq. (38) involving the time derivative of H_1 can be neglected. More precisely, this approximation is justified if the bandwidth δ_{ν} of the microwave or optical pulses is small as compared to the relevant differences between eigenfrequencies of H_0 . Through a numerical study we find that this condition is satisfied if all detunings Δ_k ($k \in \{4, 5, 6\}$) are large as compared to the bandwidth δ_{ν} . With these assumptions and for

$$\Delta_5 = \frac{|\Omega_{\text{C}}|^2}{\Delta_4}, \quad (39a)$$

$$\Delta_6 = \frac{|\Omega_{\text{A}}|^2}{\Delta_5} = \Delta_4 \frac{|\Omega_{\text{A}}|^2}{|\Omega_{\text{C}}|^2}, \quad (39b)$$

we obtain the following expressions for the coherences ϱ_{43} and ϱ_{61} ,

$$\varrho_{43} \approx i\beta\Omega_{\text{M}} + \alpha\Omega_{\text{L}}, \quad (40a)$$

$$\varrho_{61} \approx \alpha^*\Omega_{\text{M}} + ig\Omega_{\text{L}}. \quad (40b)$$

In this equation, the parameters α , β and g are defined as

$$\alpha = \frac{\Omega_{\text{C}}}{\Delta_4 \Omega_{\text{A}}^*} C_{13}, \quad (41a)$$

$$\beta = \frac{\gamma}{2} \frac{|\Omega_{\text{C}}|^2}{\Delta_4^2 |\Omega_{\text{A}}|^2} P_{33}, \quad (41b)$$

$$g = \frac{\Gamma}{2|\Omega_{\text{A}}|^2} \left(1 + 2 \frac{|\Omega_{\text{C}}|^2}{\Delta_{\text{M}}^2} \right) P_{11}. \quad (41c)$$

In the following we assume $|\Omega_{\text{R}}| \gg |\Omega_{\text{P}}|$ such that $P_{11} \approx 1$, $|C_{13}| \approx |\Omega_{\text{P}}/\Omega_{\text{R}}|$ and $P_{33} \approx |C_{13}|^2$.

Maxwell-Bloch equations

We assume that Ω_M and Ω_L propagate along the z direction. This reduces Maxwell's equations (26) to

$$\left(\frac{1}{c}\partial_t + \partial_z\right)\Omega_M = ib^2\eta_L\varrho_{43}, \quad (42a)$$

$$\left(\frac{1}{c}\partial_t + \partial_z\right)\Omega_L = i\eta_L\varrho_{61}, \quad (42b)$$

where the coherences ϱ_{43} and ϱ_{61} are given by Eq. (40). For time-independent fields Eq. (42) reduces to the following ordinary differential equation,

$$\partial_z\Omega = M\Omega, \quad (43)$$

where

$$M = \eta_L \begin{pmatrix} -b^2\beta & ib^2\alpha \\ i\alpha^* & -g \end{pmatrix}, \quad \Omega = \begin{pmatrix} \Omega_M \\ \Omega_L \end{pmatrix}. \quad (44)$$

The general solution to Eq. (43) is

$$\Omega = \exp(Mz)\Omega_0, \quad (45)$$

and Ω_0 is Ω evaluated at $z = 0$. The parameters β and g in Eq. (43) account for photon losses. In order to achieve coherent conversion with high fidelity, these terms must be small as compared to the coupling between the two fields. Formally, this requirement can be quantified by introducing the two small parameters

$$\varepsilon = \frac{b\beta}{2\alpha}, \quad (46a)$$

$$\varepsilon_\Gamma = \frac{g\gamma}{8}. \quad (46b)$$

For $\varepsilon \ll 1$ and $\varepsilon_\Gamma/\varepsilon \ll 1$, we find

$$\exp(Mz) \approx e^{-\kappa z} \begin{pmatrix} \cos(kz) & ib \sin(kz) \\ \frac{i}{b} \sin(kz) & \cos(kz) \end{pmatrix}, \quad (47)$$

where

$$k = \frac{\varepsilon}{l_{\text{abs}}}, \quad (48a)$$

$$\kappa = \frac{\varepsilon^2 + \varepsilon_\Gamma}{l_{\text{abs}}}, \quad (48b)$$

and $l_{\text{abs}} = \gamma/(4\eta_L) = 1/(\mathcal{N}\sigma_L)$ is the resonant absorption length on the $|6\rangle \leftrightarrow |1\rangle$ transition (\mathcal{N} : atomic density, σ_L : absorption cross section).

INTERACTION-INDUCED IMPERFECTIONS

In this section we discuss interaction-induced imperfections of our scheme. More specifically, we consider interactions between Rydberg atoms and interactions between a Rydberg atom and a ground state atom as possible sources of noise. Our scheme involves three Rydberg states $|3\rangle$, $|4\rangle$ and $|5\rangle$ that could contribute to

these processes. The population in state $|3\rangle$ is created through coherent population trapping induced by the auxiliary fields P and R. Since we are working in the limit $|\Omega_R| \gg |\Omega_P|$, the population in $|3\rangle$ is small. On the other hand, the population in states $|4\rangle$ and $|5\rangle$ is even smaller by several orders of magnitude as compared to the population in $|3\rangle$. It follows that the dominant source of imperfections are atoms in state $|3\rangle$. In order to analyse the detrimental effect of Rydberg-Rydberg and Rydberg-ground state interactions on our scheme, we thus focus on the impact of these processes on electromagnetically induced transparency (EIT) and coherent population trapping on the $|1\rangle \leftrightarrow |2\rangle \leftrightarrow |3\rangle$ subsystem. First, van der Waals interactions between pairs of Rydberg atoms can shift the energy of state $|3\rangle$. If this shift large or comparable to the EIT linewidth, the P field will be absorbed by atoms within the blockade radius of the Rydberg excitation [6]. Second, cooperative effects like superradiance [7] can transfer population from $|3\rangle$ to unwanted states thus destroying the coherent population trapping effect. Third, a ground state atom within the electron orbit of a Rydberg state can shift the energy of the Rydberg level [8] such that EIT is destroyed and the P field is absorbed. However, experimental results [9, 10] shows that all of these effects can be negligible in Rydberg EIT systems in the parameter regime where the probe field is much weaker than the control field such that the population of the Rydberg state is small. This is exactly the parameter regime that we are interested in, and hence our single-atom treatment can be justified. Even if interaction-induced imperfections are present, they will in the first place lead to some absorption of the P field but will not completely destroy our conversion mechanism.

In order to estimate the impact of Rydberg-Rydberg and Rydberg-ground state interactions on the detuning Δ_4 of the microwave field with the $|3\rangle \leftrightarrow |4\rangle$ transition, we note that the population in state $|3\rangle$ is typically of the order of 10^{-3} , see the parameters in Figure 2 of the main text. Complete conversion occurs at an optical density of 200 for the chosen parameters. Assuming a cold atom cloud with a length of 4.6 mm [12], this corresponds to an atom density of $1.5 \times 10^{17} \text{m}^{-3}$ and hence the Rydberg excitation density is $1.5 \times 10^{14} \text{m}^{-3}$. This corresponds to an average distance between Rydberg atoms of approximately $19 \mu\text{m}$. Based on the numbers in [13], the van der Waals shift of state $|3\rangle$ due to Rydberg-Rydberg interactions is thus roughly 0.6 Hz, 21.3 Hz and 18.7 kHz for $n = 30$, $n = 40$ and $n = 70$, respectively. These shifts are negligibly small as compared to the detuning Δ_4 of the microwave field with the $|3\rangle \leftrightarrow |4\rangle$ transition, which is of the order of several tens of MHz. Next we consider Rydberg-ground state interactions. The size of a Rydberg orbital for $n = 30$ is of the order of 200 nm. The probability for having a ground state atom within the Rydberg electron orbital for the density cited above is approximately 5×10^{-4} . Hence only a small fraction

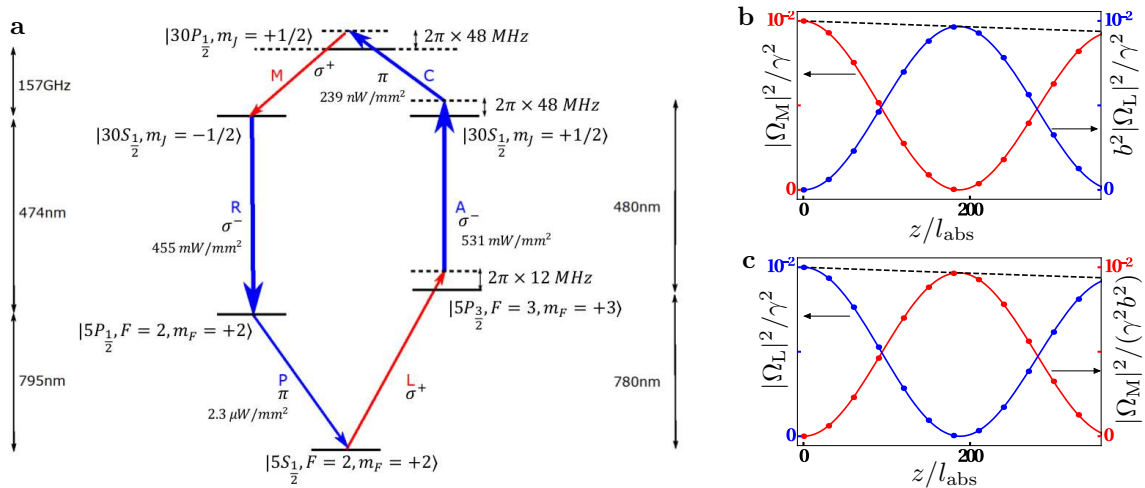


FIG. 5. **Implementation of the scheme in Rb.** **a** Realisation of the level scheme in Fig. 1c of the main text based on transitions in ^{87}Rb . All quantum numbers of the employed states as well as intensities, polarisations and detunings are indicated. Note that energy spacings are not to scale. **b** and **c** show the intensities of the microwave (red) and optical (blue) fields inside the medium for the parameters in **a**. Dots indicate the results from a numerical integration of Maxwell-Bloch equations. **b** A CW microwave field enters the medium at $z = 0$. The intensity of the microwave input field at $z = 0$ is 18.7pW/mm^2 . The intensity of the optical output field at $z = 186.8l_{\text{abs}}$ is 42.8nW/mm^2 . **c** A CW optical field enters the medium at $z = 0$. The intensity of the optical input field at $z = 0$ is 331.3nW/mm^2 . The intensity of the microwave output field at $z = 186.8l_{\text{abs}}$ is 126.7pW/mm^2 . The decay rate $\gamma = 2\pi \times 6.1\text{MHz}$ corresponds to the D_2 line. We set the decay rate Γ of all Rydberg states equal to the decay rate of the $|30S_{1/2}\rangle$ state at $T = 300\text{K}$, which is faster than the decay rate of the $|30P_{1/2}\rangle$ state. We find [11] $\Gamma/\gamma = 1/624.84$ and the ratio of the microwave and optical single-photon Rabi frequencies is $b = \sqrt{7.24}$.

of all Rydberg states will see an energy shift due to the coupling to a ground-state atom. For larger values of n , the size of the Rydberg orbital increases, but the energy shift due to the Rydberg-ground state coupling decreases. For example, for $n = 40$ the probability for having a ground state atom within the Rydberg orbital is 3×10^{-3} , and the shift is of the order of 10MHz [8]. This is already significantly smaller than the detuning of the microwave field with the $|3\rangle \leftrightarrow |4\rangle$ transition (see Section ‘Example system’).

In summary, we conclude that Rydberg-Rydberg and Rydberg-ground state interactions are a negligible perturbations to our scheme provided that the atom density and the population in $|3\rangle$ are small enough.

EXAMPLE SYSTEM

Here we present a worked example based on an atomic ensemble of ^{87}Rb atoms. The atomic level scheme is shown in the Supplementary Fig. 5a. The optical field L couples to the D_2 line, and the auxiliary P field couples to the D_1 line. The Rabi frequencies resulting from the intensities in Fig. 5a can be obtained via the transition dipole moments. For the optical transitions the corresponding data can be found in [14], and for transition dipole matrix elements between Rydberg states we employ the method outlined in [3].

Full conversion occurs after a length $l = 186.8l_{\text{abs}}$, where l_{abs} is the absorption length. For an atomic density of $\rho = 1.5 \times 10^{17}\text{m}^{-3}$, the absorption length is $l_{\text{abs}} = 2.28 \times 10^{-2}\text{mm}$, and hence full conversion occurs for a medium length of $l \approx 4.3\text{mm}$. These numbers are compatible with the experimental parameters in [12], where an even higher optical depth was achieved in a system of comparable length.

The intensities inside the medium for conversion of stationary fields is shown in the Supplementary Figs. 5b and c. The conversion efficiency at $l = 186.8l_{\text{abs}}$ is 96.7% and thus roughly identical to the conversion efficiency for the parameters of Fig. 2 in the main text.

-
- [1] M. O. Scully and M. S. Zubairy, *Quantum Optics* (Cambridge University Press, Cambridge, 1997)
 - [2] T. F. Gallagher, *Rydberg Atoms* (Cambridge University Press, Cambridge, 1994)
 - [3] T. G. Walker and M. Saffman, Phys. Rev. A **77**, 032723 (2008)
 - [4] M. Kiffner and K.-P. Marzlin, Phys. Rev. A **71**, 033811 (2005)
 - [5] M. Kiffner, U. Dorner, and D. Jaksch, Phys. Rev. A **85**, 023812 (2012)
 - [6] J. D. Pritchard and K. J. Weatherill and C. S. Adams, in *Annual Review of Cold Atoms and Molecules*, edited by K. Madison, Y. Wang, A. M. Rey, and K. Bongs, (World

- Scientific, Singapore, 2013), Vol. **1**, pp. 301.
- [7] T. Wang, S. F. Yelin, R. Cote, E. E. Eyler, S. M. Farooqi, P. L. Gould, M. Kostrun, D. Tong, and D. Vrinceanu, *Phys. Rev. A* **75**, 033802 (2007)
 - [8] V. Bendkowsky, B. Butscher, J. N. J. P. Shaffer, R. Löw, and T. Pfau, *Nature* **458**, 1005 (2009)
 - [9] K. J. Weatherill, J. D. Pritchard, R. P. Abel, M. G. Bason, A. K. Mohapatra, and C. S. Adams, *J. Phys. B* **41**, 201002 (2008)
 - [10] J. Han, T. Vogt, M. Manjappa, R. Guo, M. Kiffner, and W. Li, *Phys. Rev. A* **92**, 063824 (2015)
 - [11] I. I. Beterov, I. I. Ryabtsev, D. B. Tretyakov, and V. M. Entin, *Phys. Rev. A* **79**, 052504 (2009)
 - [12] B. Sparkes, J. Bernu, M. Hosseini, J. Geng, Q. Glorieux, P. Altin, P. Lam, N. Robins, and B. Buchler, in *Journal of Physics: Conference Series*, Vol. 467 (IOP Publishing, 2013) p. 012009
 - [13] K. Singer, J. Stanojevic, M. Weidemüller, and R. Cote, *Journal of Physics B: Atomic, Molecular and Optical Physics* **38**, S295 (Jan. 2005), ISSN 0953-4075, <http://iopscience.iop.org/0953-4075/38/2/021>
 - [14] Daniel A. Steck, “Rubidium 87 D Line Data,” available online at <http://steck.us/alkalidata> (revision 2.1.4, 23 December 2010).